Bulletin of Electrical Engineering and Informatics
Vol. 15, No. 2, April 2026, pp. 1558∼1575
ISSN: 2302-9285, DOI: 10.11591/eei.v15i2.10707

Uplink power control for multi-path channel estimation in massive multiple-input multiple-output systems

Jamal Amadid[1,2], Asma Khabba[1,3], Zakaria El Ouadi[1,3], Lahcen Sellak[4], Abdelmouttalib Bousrout[5], Abdelouhab Zeroual[1], Tole Sutikno[6]

[1]Higher Institute of Engineering and Business (ISGA), Joint Unit: UMEIT, Marrakech, Morocco
[2]I2SP Team, LISI Laboratory, Faculty of Sciences Semlalia, Cadi Ayyad University (UCA), Marrakech, Morocco
[3]Laboratory LAMIGEP, Moroccan School of Engineering Sciences (EMSI), Marrakesh, Morocco
[4]Laboratory of Complex Physical Systems (ICCPS), Higher National School of Art and Crafts, Hassan II University, Casablanca, Morocco
[5]Advanced Systems Engineering Laboratory, National School of Applied Sciences, Ibn Tofail University, Kenitra, Morocco
[6]Department of Electrical Engineering, Faculty of Industrial Technology, Universitas Ahmad Dahlan, Yogyakarta, Indonesia

Article Info

Article history:

Received May 18, 2025
Revised Dec 9, 2025
Accepted Feb 22, 2026

Keywords:

5G and 6G wireless communication systems
Massive multiple-input multiple-output
Multi-path channel estimation
Pilot contamination
Power control

ABSTRACT

Multi-path communication channels provide a realistic representation of transmitter-receiver communication in practical propagation environments. This work investigates uplink (UL) multi-path channel estimation (CE) in a massive multiple-input multiple-output (M-MIMO) multi-cell multi-user system, where each user communicates with its serving base station (BS) through a multi-path channel. The network operates using time-division duplex (TDD), exploiting channel reciprocity between the uplink and downlink. The impact of multi-path propagation on CE is analyzed using two approaches: the ideal minimum mean square error (MMSE) estimator and a proposed simplified estimator. The MMSE estimator assumes prior knowledge of the large-scale fading (LSF) coefficients of interfering users, which is impractical in real systems. To overcome this limitation, a simplified estimator is proposed that does not require such information while achieving asymptotic performance close to that of the MMSE estimator. Realistic propagation scenarios are also considered, where channels may include either non-line-of-sight (NLoS) components or a combination of line-of-sight (LoS) and NLoS paths depending on the user's distance from the BS. Furthermore, a heuristic power control strategy is introduced to mitigate pilot contamination, particularly for cell-edge users, thereby reducing inter-cell interference and improving overall system performance. Analytical and simulation results validate the proposed approach.

Corresponding Author:

Jamal Amadid
Higher Institute of Engineering and Business (ISGA), Joint Unit: UMEIT
Marrakesh, Morocco
Email: j.amadid1297@uca.ac.ma

1. INTRODUCTION

The need for high-speed data transfer, ultra-reliable connections, and the ability to support a large number of devices simultaneously has accelerated the evolution of wireless communication systems. Each new generation of mobile networks has introduced innovative technologies, ranging from advanced coding and decoding schemes to multi-antenna systems, sophisticated modulation techniques, and spectrum-efficient

protocols. Furthermore, as network usage continues to expand, encompassing applications from immersive extended reality to massive machine-type communications and autonomous systems, network architectures must evolve accordingly. This progression has led to the vision of sixth-generation (6G) networks, expected to deliver unprecedented capacity, seamless connectivity, and exceptional reliability. Following the worldwide commercialization and deployment of fifth-generation services, and in response to the need for high data rates and low latency specifications, numerous research projects on 6G networks have been launched [1]-[3].

Thanks to many new technologies, such as massive multiple-input multiple-output (M-MIMO) [4], [5], millimeter waves [6], [7], and cell-free M-MIMO [8] systems, the next generation of wireless communication systems (i.e., 6G) promise to bring considerable efficiency and flexibility to wireless networks [9]. The M-MIMO technology is a promising advancement in wireless communication networks [10], [11], leveraging hundreds of antennas at each base station (BS). These systems enable effective beamforming, enhancing communication gains by focusing signals precisely on desired areas [12], [13]. Furthermore, employing simple linear processing schemes [14], M-MIMO technology significantly improves spectral efficiency (SE) [8] and energy efficiency (EE) [15]. This improvement in SE is achieved by simultaneously serving multiple terminals over the same time-frequency resources using spatial multiplexing techniques. Conversely, enhancing energy efficiency (EE) relies on deploying a large number of antennas (NoA) at the BS [16]-[18]. Another crucial factor in optimizing the performance of M-MIMO systems is the availability of accurate channel state information (CSI), which plays a key role in detection and precoding [5], [19] at both the transmitter and the receiver. However, the reuse of pilot sequences (PSs) across frequencies in cellular networks can degrade the quality of channel estimation (CE). This phenomenon, known as pilot contamination (PC) [20]-[24], poses a bottleneck for M-MIMO technology.

Another crucial factor in optimizing the performance of M-MIMO systems is the availability of accurate CSI, which plays a vital role in both detection and precoding [5], [19]. The channel is usually experiencing multipath fading, and Rayleigh or Rician fading distributions are used to describe these effects in realistic wireless environments, depending on the presence (i.e., Rician) or absence (i.e., Rayleigh) of a dominant line-of-sight (LoS) component. Rayleigh fading models poorly scattered environments with a large number of multipaths and no LoS path; on the other hand, Rician fading considers a dominant LoS component and is suitable for circumstances where scattering is scarce. This behaviour makes even more important the need for a good channel estimator under these fading effects to get the benefits from M-MIMO. Moreover, the CSI acquisition is also very much dependent on whether time-division duplex (TDD) or frequency division duplex (FDD) duplexing is implemented. For TDD systems, when channel reciprocity is assumed, the uplink (UL) pilots can also be reused for downlink (DL) CSI estimation, which significantly lowers UL training overhead compared to FDD, where a different set of pilots and fixed assignment ratios must exist for both the DL and UL. Therefore, this attribute of TDD-based M-MIMO is very desirable for massive antenna deployments, especially when aiming for efficient and more accurate UL CE. In the literature, TDD mode is widely recognized as the optimal protocol for implementing M-MIMO systems [25], [26]. As previously said, the TDD protocol mitigates pilot overhead by leveraging channel reciprocity between the UL and DL [21], [27], [28], where pilot signals are transmitted only during the UL phase [29], [30].

Reliable data detection and effective precoding in M-MIMO systems require accurate CE. Among the estimation techniques, the least squares (LS) and minimum mean square error (MMSE) estimators are the most commonly used. The LS estimator disregards any prior statistical knowledge of the channel or noise, using only the received pilot signals to estimate the channel by minimizing squared error. While it is simple from a computational standpoint, the LS estimator is often the most inaccurate under low SNR conditions and is highly susceptible to PC. On the other hand, the MMSE estimator uses prior information of the channel, such as the channel covariance and noise variance, to minimize the mean squared error between the true channel and the estimated channel. Thus, offering improved accuracy. Especially in environments with correlated fading and limited pilot resources, the accuracy of MMSE estimation significantly exceeds that of LS estimation. However, this improvement in accuracy also involves a trade-off in terms of the computational load involved and the need for accurate channel statistics. Accordingly, the selection between LS and MMSE estimators frequently involves a trade-off between estimation performance and complexity, where the MMSE estimator is preferable in scenarios where statistical information is known and accuracy is critical. Many studies employ MMSE [31]-[33], and LS [34] estimators for CE, requiring accurate CSI at the BS. However, the MMSE estimator presupposes full knowledge of both inter-cell and intra-cell large-scale fading (LSF) coefficients, a condition that is typically impractical in real-world applications.

In the existing literature [20], [35]-[37], CE methods have extensively addressed flat fading channels, primarily focusing on orthogonal frequency-division multiplexing (OFDM) schemes. However, these approaches may not accurately reflect real-world communication environments [38]. To contextualize our research within this body of work, the following section will review recent and pertinent studies.

2. RELATED WORKS

This section reviews previous research that addresses CE and PC mitigation techniques [39]-[44]. Marzetta [16] explore the use of the LS estimator to evaluate the impact of PC in their studied systems. They find that employing orthogonal training sequences across multiple cells minimizes variations in the signal-to-interference ratio. However, relying solely on the LS estimator for CE may not yield the most effective results. Research by Jose *et al.* [18], an MMSE-based precoding technique is proposed to tackle PC in multicell M-MIMO systems. The authors solve an optimization problem by allocating orthogonal PSs to users, aiming to minimize errors for users within the serving cell and interference for users in neighboring cells. Yin *et al.* [27] explore spatially correlated channels in M-MIMO systems. They develop a CE method aided by covariance matrices, incorporating both desired and interfering channel covariances. Additionally, Bayesian methods are employed to derive two distinct channel estimators. The first estimator considered all channels in the network to the target cell, while the second focused solely on channels from users to the target cell. The authors concluded that in an ideal scenario, distinguishing between the channel covariances of desired and interference channels (i.e., covering separate subspaces) can mitigate the PC problem, especially with an increased NoA at the BS.

Shariati *et al.* [34] propose a low-complexity MMSE estimator based on polynomial expansion (PE), aiming to reduce computational complexity compared to traditional MMSE estimators. Unlike traditional MMSE estimators, which involve matrix inversions leading to cubic complexity, the proposed PE-based MMSE estimator operates with square complexity. Even with a low degree of PE, the proposed method achieves nearly optimal mean square error (MSE) performance.

Figueiredo *et al.* [35] discuss spatially correlated channels using an exponential correlation model to characterize channel correlations. An approximate MMSE estimator is introduced that relies on a sample-based covariance matrix. Its performance is strongly influenced by the quantity of samples available for estimating the actual covariance. As the sample size increases, the estimator's accuracy improves and gradually converges toward that of the Bayesian-MMSE benchmark. Özdogan *et al.* [4] investigate spatially correlated channels with Rician fading, incorporating deterministic LoS and stochastic (Non-LoS and NLoS) components. They evaluate SE using three estimators (MMSE, element-wise MMSE, and LS). The study concludes that spatial correlation enhances SE, particularly when a LoS path is available, leading to significant improvements. Albataineh *et al.* [36] explore CE in M-MIMO systems using compressive sensing and Shannon's entropy function to reduce pilot overhead. They specifically investigate DL CE under the FDD protocol, evaluating CE quality with normalized mean squared error (NMSE). However, FDD's requirement for CE in both UL and DL increases pilot overhead, limiting its suitability for M-MIMO implementation. Morales *et al.* [37] address blind CE for M-MIMO by leveraging coded data without PSs during the CE phase. They evaluate both UL and DL system performance based on signal-to-interference ratio and noise. Additionally, they propose a straightforward OFDM grid-based strategy for user allocation. However, blind CE techniques often suffer from ambiguity, reducing their attractiveness.

Arellano *et al.* [38] investigate the performance of UL spatially correlated M-MIMO Rician fading systems with particular regard to the quality of the CSI. The authors take into account model imperfections of practical CE and spatial correlation in terms of Gaussian-distributed random angles. Furthermore, the authors evaluate the performance of the MMSE channel estimator based on the normalized mean square error (NMSE) in comparison with other system configurations. Moreover, they derive an exact closed-form solution for the NMSE, which is supported by Monte Carlo simulation results. The results show that as the Rician factor decreases, which is associated with fading, the estimation accuracy tends to improve. In addition to this, greater spatial correlation, closer spacing of the antenna elements, and increased correlation improve the NMSE and, therefore, the reliability and efficiency of the overall system. However, in practical wireless environments, the presence of a LoS connection between the BS and user usually only extends to about 300 meters. Beyond this distance, the chances of maintaining LoS diminish significantly due to various obstacles and propagation conditions, resulting in predominantly NLoS channels. This has a significant effect on the accuracy of CE. However, the authors did not consider this practical aspect, as they assumed an unlimited LoS distance between

the user and the BS.

Dessie *et al.* [39] address the problem of CE and SE or cell-free M-MIMO (CF M-MIMO) systems, which offer features such as high SE, wide coverage, and effective interference suppression due to distributed antennas. Phase-aware MMSE estimators are known to provide high accuracy; however, their steep computation requirements pose a challenge. To resolve the issue, the authors propose a phase-aware element-wise MMSE (PA-EW-MMSE) estimator that employs QR decomposition jointly with a precoding matrix from the user side. Thus, the authors optimize the computation while maintaining the required and achieved performance. Authors provide both the classic phase-aware MMSE and the PA-EW-MMSE, along with closed-form expressions for UL SE, as well as energy efficiency and area throughput. However, although the authors address CE, they do not use any metric such as the MSE to evaluate system performance. Moreover, while they investigate Rician fading, in real deployments, LoS links rarely exceed 300 m [43], beyond which NLoS conditions dominate and degrade CE accuracy, a factor not addressed in the paper, which assumes an unlimited LoS range.

Many studies on CE and PC rely on the simplifying assumption that the LSF coefficients, such as path loss and shadowing of interfering cells, are perfectly known, an assumption that rarely holds in real-world multi-user M-MIMO deployments. Additionally, many of the proposed approaches for addressing PC involve algorithms with a considerable computational burden. In contrast, our work introduces and evaluates a straightforward, practically viable CE method that alleviates the PC issue without relying on prior knowledge of the LSF characteristics of interfering cells. Instead, these parameters are inferred directly from the received signal, avoiding the significant overhead associated with their explicit estimation. In addition, to better describe practical wireless environments in real deployments, the presence or absence of a LoS connection between the BS and the user depends on the distance between them. In other words, LoS conditions are highly probable for user–BS distances of less than 300 m, while distances beyond this threshold are predominantly NLoS. Thus, we introduce this practical assumption in the LSF coefficients expressions, where the LSF takes on different expressions based on the presence or absence of a LoS path between the user and its serving BS (i.e., depending on the transmitter-receiver distance). Moreover, in many scenarios, users at the cell edge suffer from significant interference due to the PC from adjacent cells. To solve this problem, we propose a power control (PoC) strategy that aims to mitigate PC issues and, therefore, enhance CE quality. Thus, the proposed heuristic PoC is designed for users located at the cell edge, who typically experience high interference from users in neighboring cells. In other words, the proposed heuristic PoC allocates higher transmission power to the users at the cell edge, compared to the user in the cell hole (i.e., close to the BS). Thus, it reduces interference from users in neighboring cells, thereby improving overall system performance.

The literature review typically assumes that studies focusing on CE and PC presume perfect knowledge of intercellular and intracellular LSF coefficients, which is often unrealistic in practical implementations. Researchers have proposed various strategies to mitigate the PC problem, but these approaches typically involve additional computational complexity, thereby increasing the overall complexity of the solutions.

2.1. Contributions

This study investigates CE and PoC in M-MIMO systems operating under a TDD protocol with a multipath channel model. The multipath channels are characterized by either NLoS conditions exclusively or a combination of LoS and NLoS paths, depending on the distance between the user and its serving BS. The primary contributions of this work are outlined below:

- We propose an efficient and straightforward strategy based on Maximum-Likelihood (ML). It is a practically viable CE method that alleviates the PC issue without relying on prior knowledge of the LSF characteristics of interfering cells. The proposed ML strategy addresses the limitations of the MMSE approach, which relies on the impractical assumption of foreknowledge of the LSF coefficients of interfering users. It is particularly effective in scenarios where communication between users and BSs occurs under either NLoS conditions or a combination of LoS and NLoS paths, depending on the user's distance from its serving BS. Moreover, these parameters are inferred directly from the received signal, avoiding the significant overhead associated with their explicit estimation.
- To better describe practical wireless environments in real deployments, the presence or absence of a LoS connection between the BS and the user depends on the distance between them. Thus, we introduce this practical assumption in the LSF coefficients expressions, where the LSF takes on two different expressions based on the presence or absence of a LoS path between the user and its serving BS (i.e., depending on the

transmitter-receiver distance). In other words, when the user–BS distance is less than 300 m, a LoS path is highly probable, whereas for distances greater than 300 m, the likelihood of having a LoS path is very low.

- In many scenarios, users at the cell edge suffer from significant interference due to the PC from adjacent cells. To solve this problem, we propose a PoC strategy that aims to mitigate PC issues and, therefore, enhance CE quality. Accordingly, the proposed heuristic PoC is designed for users located at the cell edge, who typically experience high interference from users in neighboring cells. In other words, the proposed heuristic PoC allocates higher transmission power to the users at the cell edge, compared to the user in the cell hole (i.e., close to the BS). Thus, it reduces interference from users in neighboring cells, thereby improving overall system performance.

2.2. Work-organization

Section 3 presents the system model, including the formulation of channel coefficients, LSF expressions, the pilot scheme adopted for UL CE, and the proposed PoC policy strategy. Section 4 details the CE phase, describing the estimators employed in this study. Section 5 presents the computational complexity achieved by each estimator. Section 6 reports and analyzes the simulation results, which serve to validate the theoretical framework developed in the earlier sections as well as examines, discusses, and analyzes the achieved results. Finally, section 7 concludes the paper by summarizing the main contributions and results.

3. SYSTEM MODEL

In this section, we present and describe the operational model of an M-MIMO TDD system. The model considers L hexagonally arranged contiguous cells, each containing K users with a single antenna, and a central BS that adheres to the constraints imposed by M-MIMO technology (M is much larger than K) [3], [44]. Moreover, every BS is deployed with M antennas and functions under a TDD framework, which provides notable benefits as highlighted in prior studies [16], [18], [28].

All users within each cell are served according to a time-frequency block protocol. Another critical constraint is the coherence block limitation, which determines the duration of the TDD frame based on factors such as user velocity and the number of wavelengths [11], [18], [28], [34].

To adhere to the TDD framework and synchronized-user transmission constraints, the process begins with all users in each cell transmitting their training/PSs during the UL phase. Subsequently, the BS utilizes these sequences for CE. Following this, users in all cells transmit their payload data. Using the estimated channel vectors, each BS then engages in detection and decoding schemes for UL user data and generates precoding vectors for DL data transmission.

In this study, we consider wireless channels that encompass both small-scale/fast-scale fading (SSF) and LSF coefficients. The wireless channel model assumed in our research remains static within each coherence block and is independent of factors such as the NoA at the BS, M, and users per cell, K.

We define the channel coefficients $h_{jk}^{im(p)}$, as the gain of the p-th multipath component between the k-th user in the j-th cell and the m-th antenna of the BS in the i-th cell. Thus, the vector:

$$\mathbf{h}_{jk}^{im} = \left[h_{jk}^{im(0)}, h_{jk}^{im(1)}, \ldots, h_{jk}^{im(p)}, \ldots, h_{jk}^{im(P-1)}\right] \tag{1}$$

represents the gain of all multipath component (i.e., P path) between the k-th user in the j-th cell and the m-th antenna of the BS in the i-th cell. This gain depends on both small-scale/fast-scale fading (SSF) and LSF coefficients, as expressed in (2):

$$h_{jk}^{im(p)} = \sqrt{\beta_{jk}^{i}}(g_{jk}^{im})^{(p)}, \tag{2}$$

In this context, $(g_{jk}^{im})^{(p)}$ represents the rapid amplitude-phase fluctuations of the signal, while β_{jk}^{i} denotes the signal attenuation across a broad geographical area. Assuming the propagation environment supports up to P paths, the matrix encompassing all channel vectors $\mathbf{H}_{ij}$ is structured as (3):

$$\mathbf{H}_{ij} = \begin{bmatrix} \mathbf{h}_{j1}^{i1} & \mathbf{h}_{j2}^{i1} & \ldots & \mathbf{h}_{jK}^{i1} \\ \mathbf{h}_{j1}^{i2} & \mathbf{h}_{j2}^{i2} & \ldots & \mathbf{h}_{jK}^{i2} \\ \mathbf{h}_{j1}^{i3} & \mathbf{h}_{j2}^{i3} & \ldots & \mathbf{h}_{jK}^{i3} \\ \vdots & \vdots & \ddots & \vdots \\ \mathbf{h}_{j1}^{iM} & \mathbf{h}_{j2}^{iM} & \ldots & \mathbf{h}_{jK}^{iM} \end{bmatrix} \tag{3}$$

This matrix represents the collective channel responses linking the K users in the j_{th} cell to the M antennas of the BS located in the i_{th} cell (i.e., $\mathbf{H}_{ij} = [\mathbf{H}^i_{j1}, \mathbf{H}^i_{j2}, \ldots, \mathbf{H}^i_{jK}]$), where $\{i, j\} = 1, \ldots, L$.

Multipath propagation characterizes realistic wireless communication environments, especially in urban microcell scenarios where dense building structures are common and the spacing between BSs generally remains below one kilometer, as highlighted in [43]. These multipath channels predominantly exhibit Small-Scale or Fast Fading phenomena [43], which are affected by propagation delays, relative motion, and spatial variations between transmitters and receivers.

This study aims to explore and analyze a multi-path channel model that incorporates LSF with two expressions based on whether there is LoS or NLoS propagation. The presence of LoS and NLoS paths depends on the distance between the user and the BS, as outlined in the 3GPP model provided in [43]. In particular, the LoS link is limited by a threshold distance, beyond which it cannot be sustained. Thus, depending on the environment, one can identify a region where only NLoS propagation occurs and another region where both LoS and NLoS components are simultaneously present. The probability of LoS occurrence is determined by the user's distance from its serving BS (4):

$$Pr(LoS) = \begin{cases} \frac{300 - d^i_{jk}}{300}, & d^i_{jk} \in (0, 300), \\ 0, & d^i_{jk} > 300. \end{cases} \tag{4}$$

The presence of LoS or NLoS paths directly affects the LSF coefficient. Specifically, when a LoS path exists between the transmitter and receiver, the corresponding LSF coefficient in decibels (dB) is expressed as (5):

$$\beta^i_{jk} = -30.18 - 10\alpha^{LoS} log_{10}(d^i_{jk}) + \Upsilon^i_{jk}, \tag{5}$$

Here, $\Upsilon^i_{jk} \sim \mathcal{N}_{\mathcal{C}}\big(0, (\sigma^{\mathrm{LoS}}_{sf})^2\big)$ represents the shadowing (shadow fading) component, where $\sigma^{\mathrm{LoS}}_{sf} = 4$ indicates the standard deviation of the random fluctuations. In the absence of a LoS path between the transmitter and receiver, the corresponding LSF coefficient is expressed in decibels (dB) as (6):

$$\beta^i_{jk} = -34.53 - 10\alpha^{NLoS} log_{10}(d^i_{jk}) + \Psi^i_{jk}, \tag{6}$$

Here, $\Psi^i_{jk} \sim \mathcal{N}_{\mathcal{C}}(0, (\sigma^{NLoS}_{sf})^2)$ represents the shadow fading, where $\sigma^{NLoS}_{sf} = 10$.

3.1. Uplink training phase

In this section, we focus on pilot-based estimation [3], [4], [6]. During this phase, users in each cell transmit pilot or training sequences to communicate with their respective BS.

Assuming a frequency reuse factor of one across cells (due to limited coherence blocks) represents the worst-case scenario, leading to significant PC, which acts as a bottleneck for M-MIMO systems even under conditions where the NoA at the BS approaches infinity. Additionally, we consider synchronized timing among cells. These assumptions collectively represent the most challenging conditions for M-MIMO [16]. Therefore, the PS transmitted by the k_{th} user is formulated as (7):

$$\phi_k = [\,\varphi_k(0), \ldots, \varphi_k(S-1)] \tag{7}$$

Here, S denotes the length of the PSs. For the considered multi-path channel model, it is assumed that each user-to-BS antenna connection propagates through P distinct paths. The interaction between the PS of the k_{th} user and the M propagation channels linking that user to a given BS can be formulated in matrix notation as (8):

$$\Phi_k = \begin{bmatrix} \varphi_k(0) & \varphi_k(S-1) & \ldots & \varphi_k(S-P+1) \\ \varphi_k(2) & \varphi_k(1) & \ldots & \varphi_k(S-P+3) \\ \vdots & \vdots & \ddots & \vdots \\ \varphi_k(S-1) & \varphi_k(S-2) & \ldots & \varphi_k(S-P+S) \end{bmatrix} \tag{8}$$

This matrix (denoted as $\Phi_k \in \mathbb{C}^{S \times P}$) is constructed using a PS circularly shifted by the k_{th} user. According to literature references (section 7 in [20]), each element of this matrix can be computed as (9):

$$\varphi_k(s) = exp(-i\pi f \frac{s(s+1)}{S}), \quad s = 0, 1, 2, \ldots, S-1 \tag{9}$$

Here, f represents the sequence index, which must be chosen such that it is relatively prime to the PS length S, with s ranging from 0 to $S-1$.

The matrix defined in (8) satisfies the orthogonality condition $\Phi_k^H \Phi_k = S\mathbf{I}_P$. Importantly, within the framework of cyclically shifted sequences, these pilot sequences remain mutually orthogonal [20].
Moreover, a composite matrix comprising the pilot sequences of all K users, denoted by $\mathbf{\Phi} \in \mathbb{C}^{S \times KP}$, can be expressed as (10):

$$\mathbf{\Phi} = [\,\Phi_1, \Phi_2, \ldots, \Phi_K] \tag{10}$$

Indeed, each of the K users within each cell must utilize orthogonal PSs relative to the other users (meaning the length of the PSs must exceed the product of the number of users per cell and the number of paths, $S > KP$). This approach ensures that intra-cell interference is not addressed in this study. As mentioned earlier, the length S of the PSs should ideally be a prime number close to $K \times P$.

When $S > KPL$ is satisfied, the system is guaranteed not to encounter PC issues. Each user employs a distinct PS that is orthogonal to all other sequences used in the network, though practical limitations due to the coherence block constraint are acknowledged. Consequently, the BS in the i_{th} cell receives the signal $Y \in \mathbb{C}^{M \times S}$, which can be expressed as (11):

$$\mathbf{Y}_i = \sum_{j=1}^{L} \sum_{k=1}^{K} \sqrt{q}_{jk} \mathbf{H}_{jk}^i \Phi_k^T + W_i \tag{11}$$

In this expression, q_{jk} indicates the transmit power assigned to the k_{th} user within the j_{th} cell, and $W_i \in \mathbb{C}^{M \times S}$ represents the noise matrix at the i_{th} BS, with each entry of W_i modeled as a circularly symmetric complex Gaussian random variable, $\mathcal{C}_{\mathcal{N}}(0,1)$.

Prior to initiating the CE process, (11) can be reformulated independently of the pilot sequences, so that it depends exclusively on the channel matrices and noise components, as shown (12):

$$\mathbf{y}_{ik} = \mathbf{Y}_i \Phi_k^* = S \sum_{j=1}^{L} \sqrt{q_{jk}} \mathbf{H}_{jk}^i + b_{ik} \tag{12}$$

Here, $b_{ik} = W_i \Phi_k^*$ (in $\mathbb{C}^{M \times 1}$) follows a complex normal distribution $\mathcal{N}_{\mathcal{C}}(0M \times 1, \mathbf{I}_M)$.

3.2. Proposed heuristic power control

In this subsection, the proposed heuristic PoC scheme is designed to address the worst-case scenario, where users are located at the cell edge. In such cases, users experience a significantly higher degree of PC due to increased interference from adjacent cells. To mitigate this issue, we introduce a PoC strategy that aims to reduce PC and consequently improve CE quality. The proposed heuristic PoC approach assigns higher transmission power to cell-edge users compared to those located near the BS (i.e., within the cell center). This power allocation strategy helps suppress interference from users in neighboring cells, thereby enhancing overall system performance. The transmit power allocated to the k_{th} user in the i_{th} cell is given by (13):

$$q_{ik} = \begin{cases} q^{max}, & \chi > \frac{\beta_{ik}^i}{\beta_{i,min}^i}, \\ q^{max} \chi \frac{\beta_{i,min}^i}{\beta_{ik}^i}, & \chi \leq \frac{\beta_{ik}^i}{\beta_{i,min}^i}, \end{cases} \tag{13}$$

Here, $\beta_{i,min}^i$ defines the smallest LSF value provided by a user in the i_{th} cell being served by the BS in the same cell. Hence, $\beta_{i,min}^i$ can be expressed as (14):

$$\beta_{i,min}^i = min(\beta_{i,1}^i, \ldots, \beta_{i,K}^i) \tag{14}$$

The proposed strategy (as provided in (13)) allows a user with the poorest channel conditions to transmit at maximum power. Additionally, with the threshold χ set to 10 dB, the strategy ensures that other users limit their transmission power to comply with the SNR constraints (i.e., the signal-to-noise ratio cannot exceed 10 dB). Furthermore, the maximum transmission power q^{max} is set at 10 dBm, as referenced in [28].

4. CHANNEL ESTIMATION PROCESS

To estimate the channel $\mathbf{H_{ik}^{i}}$ at the i_{th} BS (i.e., i_{th} cell), a straightforward technique is employed as referenced in [38], and it is represented as (15):

$$(\hat{\mathbf{H}}_{\mathbf{ik}}^{\mathbf{i}})^{\mathbf{LS}} = \boldsymbol{\lambda}_{ik} = \frac{\mathbf{y}_{ik}}{\sqrt{q_{ik}}S} = \mathbf{H_{ik}^{i}} + \sum_{j\neq i}^{L} \sqrt{\frac{q_{jk}}{q_{ik}}} \mathbf{H_{jk}^{i}} + \frac{b_{ik}}{\sqrt{q_{ik}}S} \tag{15}$$

Here, $\boldsymbol{\lambda}_{ik} \in \mathbb{C}^{M\times P}$ (also known as the LS-based channel estimate $(\hat{\mathbf{H}}_{\mathbf{ik}}^{\mathbf{i}})^{\mathbf{LS}}$ [35]) is a matrix representing the estimated version of the channel $\mathbf{H_{ik}^{i}}$ at the i_{th} BS using a conventional method. Additionally, each column of $\boldsymbol{\lambda}_{ik}$ is normally distributed as $\mathcal{C}_{\mathcal{N}}(0_M, \Lambda_{ik}\mathbf{I_M})$.

$$\Lambda_{ik} = \sum_{j=1}^{L} \frac{q_{jk}}{q_{ik}} \beta_{jk}^{i} + \frac{1}{q_{ik}S} \tag{16}$$

It is important to note that Λ_{ik} incorporates the LSF coefficients from all users sharing the same PS across different cells, in addition to a parameter representing the inverse of the noise power.

4.1. Minimum mean square error channel estimation

The Bayesian-MMSE estimator assumes prior knowledge of all LSF coefficients for users, which is impractical in real-world implementations [38]. Since the i_{th} BS does not possess prior knowledge of the LSF coefficients for the k_{th} user in the j_{th} cell ($\{i, j\} = 1, \ldots, L$, with $i \neq j$) [20], [32], the expression for the estimated channel coefficient using the MMSE estimator is formulated as (17):

$$(\hat{\mathbf{H}}_{\mathbf{ik}}^{\mathbf{i}})^{\mathbf{mmse}} = \frac{\beta_{ik}^{i}}{\Lambda_{ik}} \boldsymbol{\lambda}_{ik} = \frac{\beta_{ik}^{i}}{\Lambda_{ik}} (\hat{\mathbf{H}}_{\mathbf{ik}}^{\mathbf{i}})^{\mathbf{LS}} \tag{17}$$

Each column of the estimated channel gain $(\hat{\mathbf{H}}_{\mathbf{ik}}^{\mathbf{i}})^{\mathbf{mmse}}$ follows a normal distribution, denoted as $\mathcal{N}_{\mathcal{C}}(0_M, \frac{(\beta_{ik}^{i})^2}{\Lambda_{ik}}\mathbf{I}_M)$.

On the other hand, MSE is the metric employed to calculate and assess the CE error. Hence, the MSE expression for ideal MMSE is formulated as (18):

$$\begin{aligned} MSE_{ik}^{mmse} = \frac{1}{MP} Tr\left\{ \mathbb{E}\{\| (\tilde{\mathbf{H}}_{\mathbf{ik}}^{\mathbf{i}})^{\mathbf{mmse}}\|^2\} \right\}, &= \frac{1}{MP} Tr\left\{ \mathbb{E}\{\|\mathbf{H}_{ik}^{i} - (\hat{\mathbf{H}}_{\mathbf{ik}}^{\mathbf{i}})^{\mathbf{mmse}}\|^2\} \right\}, \\ &= \beta_{ik}^{i}(1 - \frac{\beta_{ik}^{i}}{\Lambda_{ik}}) \end{aligned} \tag{18}$$

Here, $(\tilde{\mathbf{H}}_{\mathbf{ik}}^{\mathbf{i}})^{\mathbf{mmse}}$ represents the estimation error. On the other hand, it is evident that the performance of the ideal MMSE is significantly influenced by the UL power q_{ik}, the intended LSF β_{ik}^{i}, and the level of inter-cell interference.

4.2. Proposed channel estimation

The Bayesian-MMSE estimator relies on assumptions that are challenging to implement in a realistic setting. Therefore, to address this limitation, a novel estimator is proposed based on the ML approach, ensuring an unbiased estimation ($\mathbb{E}\{\hat{X}\} = X$) as discussed in [20]. This new estimator focuses on estimating Λ_{ik} instead of β_{ik}^{i}, reducing complexity compared to the MMSE estimator, which estimates individual LSF coefficients. The estimated coefficient $\hat{\Lambda}_{ik}$ denoted in (16), leverages the ML estimator and maintains unbiasedness ($\mathbb{E}\{\hat{\Lambda}_{ik}\} = \Lambda_{ik}$). It is expressed as a function of $\boldsymbol{\lambda}_{ik}$, the NoA at the BS M and the number of paths P, as (19):

$$\hat{\boldsymbol{\lambda}}_{ik} = \frac{\|\boldsymbol{\lambda}_{ik}\|_F^2}{MP} \tag{19}$$

Here, $\| \bullet \|_F^2$ denotes the Frobenius norm, where $\|\boldsymbol{\lambda}_{ik}\|_F^2 = Tr(\boldsymbol{\lambda}_{ik}^H \boldsymbol{\lambda}_{ik})$, and $Tr(\bullet)$ represents the trace operator. It is given that $\mathbb{E}\{\boldsymbol{\lambda}_{ik}^H \boldsymbol{\lambda}_{ik}\} = M\Lambda_{ik}\mathbf{I}_P$. According to (19), $M\hat{\Lambda}_{ik} = \frac{|\boldsymbol{\lambda}_{ik}|_F^2}{P}$. As P increases, the

expression $\frac{|\boldsymbol{\lambda}_{ik}|_F^2}{P}$ converges more quickly to the actual value $M\Lambda_{ik}$. By substituting Λ_{ik} with the estimated value ($\hat{\Lambda}_{ik}$) in the MMSE estimator expression, we derive the expression for the proposed estimator as (20):

$$(\hat{\mathbf{H}}_{\mathbf{ik}}^{\mathbf{i}})^{\mathbf{Proposed}} = MP\frac{\beta_{ik}^i}{\|\boldsymbol{\lambda}_{ik}\|_F^2}\boldsymbol{\lambda}_{ik} \tag{20}$$

According to (20), the proposed estimator is influenced by the NoA at the BS and the number of paths per channel, unlike the ideal MMSE estimator.
Simulations in the following section demonstrate that an asymptotic result is achieved as either M or P increases.
It is crucial to emphasize that when there is only one path per channel, $P = 1$, (20) simplifies to (8) in [35]. An approximate expression of the MSE for the proposed estimator is provided in (21):

$$\begin{aligned} MSE_{ik}^{Proposed} &= \frac{1}{M \times P} Tr\left\{\mathbb{E}\{\|(\tilde{\mathbf{H}}_{\mathbf{ik}}^{\mathbf{i}})^{\mathbf{Proposed}}\|^2\}\right\}, \\ &= \frac{1}{M \times P} Tr\left\{\mathbb{E}\{\|\mathbf{H}_{ik}^i - (\hat{\mathbf{H}}_{\mathbf{ik}}^{\mathbf{i}})^{\mathbf{Proposed}}\|^2\}\right\}, \\ &\approx \beta_{ik}^i\left[1 - \frac{\beta_{ik}^i(MP-2)}{\Lambda_{ik}(MP-1)}\right] \end{aligned} \tag{21}$$

The effectiveness of the proposed estimator, as evaluated using the MSE metric, is significantly influenced by the UL power q, the desired LSF β_{ik}^i, the NoA at the BS, M, the number of paths per channel, P, and the level of inter-cell interference.

To derive the approximate analytical MSE expression for the proposed channel estimator. Thus, we first introduce 3 supporting lemmas.
Lemma 1: let $Z_n \sim \mathcal{C}_{\mathcal{N}}(0, \sigma_z^2)$ for all n, where the variables are independent. Then:

$$\sum_{n=1}^{M} |Z_n|^2 \sim \Gamma(M, \sigma^2) \tag{22}$$

where $\Gamma(\cdot)$ denotes the Gamma distribution.
Lemma 2: if $Y \sim \Gamma(c, \phi)$ and $1/Y$ follows the inverse-Gamma distribution $\Gamma^{-1}(c, \phi)$, then:

$$\mathbb{E}\left[\frac{1}{Y}\right] = \frac{1}{\phi(c-1)}. \tag{23}$$

Lemma 3: consider two random variables Z and F with means μ_Z and μ_F, variance σ_Z^2 for Z, and covariance σ_{ZF} between them. An approximation for the expectation of the ratio Z/F is given by:

$$\mathbb{E}\left[\frac{Z}{F}\right] \approx \frac{\mu_Z}{\mu_F} - \frac{\sigma_{ZF}}{\mu_F^2} + \frac{\mu_Z}{\mu_F^3}\sigma_F^2. \tag{24}$$

Proof: for a bivariate function $h(z, f)$, the second-order Taylor expansion around the point (x, y) is:

$$\begin{aligned} h(z,f) &= h(x,y) + h_z(x,y)(z-x) + h_f(x,y)(f-y) \\ &\quad + \frac{1}{2}\left[h_{zz}(x,y)(z-x)^2 + 2h_{zf}(x,y)(z-x)(f-y) + h_{ff}(x,y)(f-y)^2\right], \end{aligned} \tag{25}$$

where the subscripts denote partial derivatives. In our situation, for $h(Z, F) = Z/F$, we have:

$$h_z = \frac{1}{F}, \quad h_{zz} = 0, \quad h_f = -\frac{Z}{F^2}, \quad h_{ff} = \frac{2Z}{F^3}, \quad g_{zf} = -\frac{1}{F^2}. \tag{26}$$

Substituting these derivatives into the Taylor expansion and expanding around (μ_Z, μ_F) yields:

$$\frac{Z}{F} \approx \frac{\mu_Z}{\mu_F} - \frac{\mu_Z}{\mu_F^2}(Y-\mu_F) + \frac{1}{\mu_F}(Z-\mu_Z) + \frac{1}{2}\left[\frac{2\mu_Z}{\mu_F^3}(F-\mu_F)^2 - \frac{2}{\mu_F^2}(F-\mu_F)(Z-\mu_Z)\right]. \tag{27}$$

Finally, applying and simplifying the expectation operator to this expression gives the approximation stated in Lemma 3.

A. Proof of the approximate MSE, $MSE_{ik}^{Proposed}$

To facilitate the derivation, the de-spread vector $\boldsymbol{\lambda}_{ik}$ can be represented as the matrix:

$$\boldsymbol{\lambda}_{ik} = \begin{bmatrix} \lambda_{ik1}^{(0)} & \lambda_{ik1}^{(1)} & \cdots & \lambda_{ik1}^{(P-1)} \\ \lambda_{ik2}^{(0)} & \lambda_{ik2}^{(1)} & \cdots & \lambda_{ik2}^{(P-1)} \\ \vdots & \vdots & \ddots & \vdots \\ \lambda_{ikM}^{(0)} & \lambda_{ikM}^{(1)} & \cdots & \lambda_{ikM}^{(P-1)} \end{bmatrix}, \tag{28}$$

where each element:

$$\lambda_{ikm}^{(p)} = \sum_{l=1}^{L} h_{ilkm}^{(p)} + b_{ikm}^{(p)} \sim \mathcal{C}_{\mathcal{N}}(0, \Lambda_{ik}), \quad \forall p. \tag{29}$$

Note that the squared Frobenius norm of $\boldsymbol{\lambda}_{ik}$,

$$\|\boldsymbol{\lambda}_{ik}\|_F^2 = \sum_{m=1}^{M} \sum_{p=0}^{P-1} |\lambda_{ikm}^{(p)}|^2, \tag{30}$$

is a positive scalar random variable. The approximate MSE $MSE_{ik}^{Proposed}$ can be expanded as:

$$\begin{aligned} MSE_{ik}^{Proposed} = & \frac{1}{MP}\mathbb{E}\left[\mathrm{Tr}\left((\hat{\mathbf{H}}_{ik}^{i})^{Proposed}((\hat{\mathbf{H}}_{ik}^{i})^{Proposed})^{H}\right)\right] \\ & + \frac{1}{MP}\mathbb{E}\left[\mathrm{Tr}\left(\mathbf{H}_{ik}^{i}(\mathbf{H}_{ik}^{i})^{H}\right)\right] - \frac{2}{MP}\mathbb{E}\left[\mathrm{Tr}\left(\mathfrak{Re}\left\{(\hat{\mathbf{H}}_{ik}^{i})^{Proposed}((\mathbf{H}_{ik}^{i}))^{H}\right\}\right)\right] \end{aligned} \tag{31}$$

Using Lemma 1, the norm $\|\boldsymbol{\lambda}_{ik}\|_F^2$ follows a Gamma distribution $\Gamma(MP, \Lambda_{ik})$. Applying Lemma 2 yields:

$$\mathbb{E}\left[\frac{1}{\|\boldsymbol{\lambda}_{ik}\|_F^2}\right] = \frac{1}{\Lambda_{ik}(MP-1)}. \tag{32}$$

Hence, the first expectation term evaluates to:

$$\frac{1}{MP}\mathbb{E}\left[\mathrm{Tr}\left((\hat{\mathbf{H}}_{ik}^{i})^{Proposed}((\hat{\mathbf{H}}_{ik}^{i})^{Proposed})^{H}\right)\right] = \frac{MP(\beta_{ik}^{i})^2}{\Lambda_{ik}(MP-1)}. \tag{33}$$

The second term simplifies to:

$$\frac{1}{MP}\mathbb{E}\left[\mathrm{Tr}\left(\mathbf{H}_{ik}^{i}(\mathbf{H}_{ik}^{i})^{H}\right)\right] = \beta_{ik}^{i}. \tag{34}$$

For the third term, direct evaluation is complex due to the ratio of random variables. Using a second-order Taylor series approximation (Lemma 3), we approximate:

$$-\frac{2}{MP}\mathbb{E}\left[\mathrm{Tr}\left(\mathfrak{Re}\left\{(\hat{\mathbf{H}}_{ik}^{i})^{Proposed}(\mathbf{H}_{ik}^{i})^{H}\right\}\right)\right] \approx -\frac{2(\beta_{ik}^{i})^2}{\Lambda_{ik}}. \tag{35}$$

Substituting these results back completes the proof of the approximate MSE expression.

Final MSE

The approximate MSE is:

$$MSE_{ik}^{Proposed} \approx \frac{MP(\beta_{ik}^{i})^2}{\Lambda_{ik}(MP-1)} + \beta_{ik}^{i} - \frac{2(\beta_{ik}^{i})^2}{\Lambda_{ik}} = \beta_{ik}^{i}\left[1 - \frac{\beta_{ik}^{i}(MP-2)}{\Lambda_{ik}(MP-1)}\right] \tag{36}$$

The paragraph below summarizes the parameter values used in the simulations for this study. The parameter values utilized for the simulation are summarized as Table 1. The network consists of 7 cells (L),

each cell accommodating 10 users (K). The BSs are equipped with 30 antennas (M), with a fixed length of PSs (S) set to 223. Each channel includes 20 paths (P), and the cell hole size is 50 meters. The cell radius in micro-urban environments, according to [43], is 500 meters. The sequence index (f) used is 119. The path-loss exponent for LoS communication is 2.6 (α^{LoS}), while for NLoS it is 3.8 (α^{NLoS}). The standard deviation of shadowing effects for LoS and NLoS paths is 4 (σ^{LoS}) and 10 (σ^{NLoS}), respectively.

The system simulation is conducted using MATLAB version 2019. The scenario involves seven hexagonal-shaped cells with single-antenna users uniformly distributed across the coverage area. Each BS is equipped with a uniform linear array. The cell radius is set to 500 meters in a micro-urban environment [43]. Communication between users and BSs considers either NLoS paths exclusively or a combination of LoS and NLoS paths, determined by (5) and (6). The presence or absence of the LoS path significantly impacts path-loss and shadowing values (i.e., LSF coefficients), which are averaged over $10,000$ $realizations$. Channel gains and CE are computed based on whether the LoS path is present, with CE performance assessed using the MSE metric. In addition, the proposed heuristic PoC scheme allocates transmission power based on the user's location within the cell (i.e., at the cell edge or near the cell center). Specifically, users situated at the cell edge are assigned higher transmission power compared to those located closer to the BS. This location-aware power allocation strategy effectively mitigates interference from users in adjacent cells, thereby improving the overall system performance.

Table 1. Summary of simulation parameters

Parameter	Description	Value/range
L	Number of cells	7
S	PS length	223
P	number of multipath per channel	20
M	NoA at each BS	30
K	Number of users per cell	10
$q_{\max}$	Maximum transmit power	10 dbm
χ	threshold factor	10 db
W_i	noise matrix associated with the i_{th} BS	$\in \mathbb{C}^{M \times S}$
σ_{sf}^{LoS}	Standard deviation of shadowing effects for LoS	4
σ_{sf}^{NLoS}	Standard deviation of shadowing effects for NLoS	10
α_{sf}^{NLoS}	Path-loss exponent for NLoS	3,8
α_{sf}^{LoS}	Path-loss exponent for LoS	2,6
-	Frequency reuse pattern	1
-	Number of Monte Carlo simulation trials	10000

5. COMPUTATIONAL COMPLEXITY

Algorithmic complexity measures how the number of elementary operations of an algorithm grows with problem size. For example, in large-scale systems, such as CE in M-MIMO, the most prominent operations involve matrix multiplication, matrix factorization or inversion, and scalar multiplication of matrices. In this section, we focus on the computational complexity provided through different estimators, i.e., the LS estimator (computational complexity of $\mathcal{O}(n^2)$), MMSE estimator, and the proposed estimators, as shown in Table 2). The complexity is primarily a function of the parameters S, P, M, L, K, and the number of iterative steps.

Table 2. Comparison of estimators in terms of complexity and performance

Estimator	Estimation accuracy	Computational complexity	Noise robustness
LS	Moderate	$\mathcal{O}(n^2)$	Low
MMSE	High	$\mathcal{O}(n^3)$	High
Proposed estimator	High/moderate	$\mathcal{O}(n)$–$\mathcal{O}(n^2)$	Moderate–high

Thus, in our work, the MMSE estimator is commonly used in CE due to its superior accuracy compared to the conventional LS estimator. Still, even with the improvements provided by the MMSE estimator, it is known to have higher computational complexity compared to the LS estimator. The computational complexity of the MMSE estimator is driven mainly by the pilot signals and the channel covariance matrices. Specifically, for the MMSE estimation, the inversion of an $S \times S$ matrix is required, with S being the pilot length, which is often on the order of $K \times P$, where K is the number of users and P is the number of paths.

This pilot length scaling is of cubic order (i.e., $(\mathcal{O}(n^3))$), which makes the complexity of this matrix inversion step computationally expensive.

On the other hand, the proposed estimator achieves a computational complexity of $(\mathcal{O}(n))$ to $(\mathcal{O}(n^2))$ by avoiding full matrix inversion and taking advantage of the structure in the covariance and pilot matrices. This makes it more suitable for the real-time, large-scale M-MIMO system requirements compared to the MMSE estimator, which operates at $\mathcal{O}(n^3)$ complexity. It achieves a computational complexity scaling between $(\mathcal{O}(n))$ and $(\mathcal{O}(n^2))$, giving a marked improvement over the MMSE processing time, real-time performance in M-MIMO systems, and resilience to noise, making it adequate in practical settings. This makes it particularly suitable for systems with low latency.

6. RESULTS AND DISCUSSION

We simulate a multi-cell, multi-user scenario with hexagonal-shaped cells, where users are uniformly distributed across the cells. In addition, each BS is centrally located within each cell. The parameter values used for simulation are detailed above.

This section aims to validate the theoretical expressions presented earlier through simulation figures. Moreover, during this section, we compare simulated and analytical results across various scenarios. In our study, we employ two estimators for CE: the Bayesian-MMSE estimator and our proposed ML estimator. Furthermore, we evaluate the performance of the proposed estimator under diverse conditions (such as SNR, NoA at the BS, number of paths), focusing on the communication link between users and their serving BSs. This link can be established using either NLoS paths exclusively or both LoS and NLoS paths, depending on factors such as environmental conditions and user-to-BS distance. The presence or absence of a LoS path notably impacts path loss and shadowing, which in turn influence the LSF coefficients embedded in our model. Therefore, the LSF model exhibits significant variations in its behavior. Notably, LSF coefficients are averaged over $10,000\ realizations$ to ensure robustness and accuracy in our simulations. Depending on the presence or absence of a LoS path between the user and its serving BS, different LSF coefficients are applied to compute the estimated channel vector. If a LoS path exists, characterized by path-loss exponent α^{LoS} and shadowing standard deviation σ_{sf}^{LoS} (5), it is utilized. Conversely, if only NLoS paths exist, characterized by α^{NLoS} and σ_{sf}^{NLoS} (6), those coefficients are applied.

Following the specification of simulation parameters and the selection of an appropriate LSF model for each scenario, it is observed that the likelihood of a LoS path is predominantly determined by the distance between the user and its associated BS. Specifically, when the distance is less than 300 meters, the user can benefit from a LoS path, as outlined in [43]. Beyond this threshold, LoS communication is not possible. Throughout this segment, we present and compare analytical and simulated results for each estimator under different scenarios, where the quality of CE is evaluated using the MSE metric. Figure 1 illustrates the MSE as a function of the SNR. The MSE metric is utilized to evaluate the performance of both the conventional MMSE estimator and the proposed estimator. As shown in the figure, the MMSE estimator demonstrates superior performance compared to the proposed method. Additionally, to assess the estimation quality of the proposed estimator, various averages of the diagonal elements of the matrix $\boldsymbol{\lambda}_{ik}^H \boldsymbol{\lambda}_{ik}$ are considered.

Figure 1 demonstrates that the performance of the proposed estimator is strongly influenced by the number of averaged elements (NoAE) employed in the estimation process. Specifically, a smaller NoAE leads to a larger MSE gap between the proposed estimator and the conventional MMSE estimator. This gap significantly decreases as the NoAE increases. For example, at an SNR of 30 dB, the MMSE estimator achieves an MSE of 3.4×10^{-3}, while the proposed estimator, when averaging over 20 elements, attains an MSE of 3.7×10^{-3}. Moreover, both analytical and simulation-based results are provided for each estimator to validate their performance. The results depicted in the figure indicate that the analytical and simulated results perform similarly, thereby confirming the accuracy and reliability of the proposed analytical framework.

Figure 2 is presented to evaluate the impact of the NoA at the BS on the performance of the proposed estimator, highlighting the dependency of its effectiveness on the selected NoAE. The figure illustrates the MSE as a function of the NoA at the BS, denoted by M. The estimation performance of the proposed method is compared against that of the conventional MMSE estimator. As expected, the MMSE estimator consistently achieves superior accuracy compared to the proposed estimator. The evaluation of the proposed estimator is conducted by averaging different numbers of components extracted from the main diagonal of the matrix $\boldsymbol{\lambda}_{ik}^H \boldsymbol{\lambda}_{ik}$, reflecting the influence of NoAE on estimation quality. Moreover, the choice of NoAE has a significant

impact on the performance of the proposed estimator. A smaller NoAE leads to a larger MSE gap between the proposed estimator and the conventional MMSE estimator. This gap becomes even more pronounced when the NoA at the BS (i.e., M) is small. However, as both NoAE and M increase, the performance gap between the two estimators gradually decreases. Notably, the proposed estimator achieves performance comparable to that of the MMSE estimator when the NoAE is equal to the number of multipath components. For example, when the NoA at the BS M exceeds 80, averaging over 5, 10, or 20 elements yields MSE results that closely approximate those of the MMSE estimator.

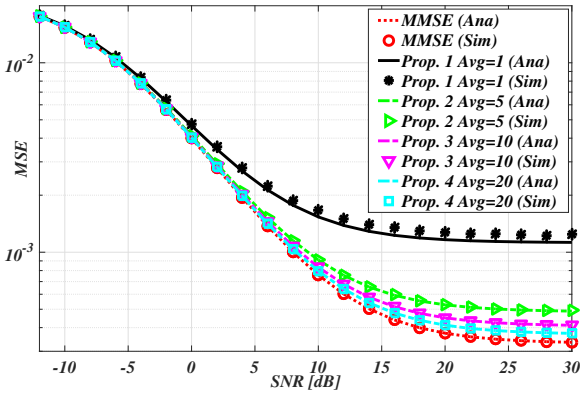

Figure 1. MSE as a function of $SNR\,(dB)$

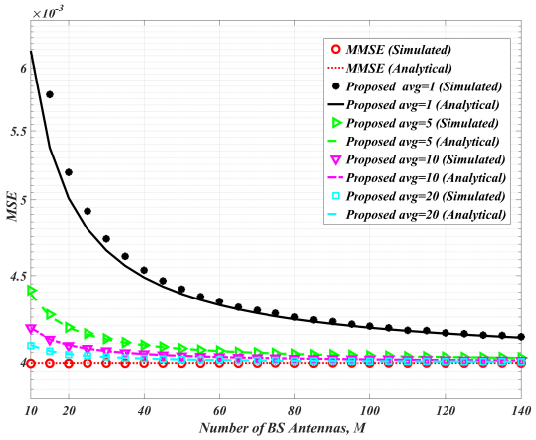

Figure 2. MSE as a function of the number of BS antennas, M

Figure 2 also presents both analytical and simulated results for each estimator, demonstrating a high degree of consistency between the two approaches. Notably, scenarios involving smaller NoAEs exhibit a closer match between analytical and simulated results, which can be attributed to the reduced complexity introduced by the limited number of averaged elements.

Figure 3 illustrates the MSE metric as a function of the number of multi-paths, P, and the PS length, S, for both the MMSE estimator and the proposed estimator, with an SNR set to 20 dB. This figure aims to validate the theoretical requirement $S \geqslant KP$, indicating that an increase in P necessitates longer PSs to maintain orthogonality among sequences serving K users. The effectiveness of the proposed estimator correlates strongly with the NoA at the BS and the chosen number of multi-paths, adhering to coherence block constraints. As the NoA at the BS M increases, the performance of the proposed estimator improves significantly. As shown in Figure 3, the MMSE estimator consistently achieves lower MSE values than the proposed estimator across all values of P. However, for $P > 46$, the proposed estimator yields performance comparable to that of the MMSE estimator, particularly when $M = 30$ or $M = 100$. Furthermore, analytical and simulated results are provided for each estimator, demonstrating a high degree of consistency between the two results and thereby validating the accuracy of the proposed analytical model.

Figure 4 depicts the CE MSE performance when the LSF coefficients β_{lk}^{i} are randomly generated. In this evaluation, the NoA at the BS is fixed at $M = 30$. The MSE metric is employed to assess the performance of both the conventional MMSE estimator and the proposed estimator. The reported MSE values are averaged over 10,000 independent realizations of $\{\beta_{lk}^{i}\}$. As shown in the figure, the MMSE estimator exhibits superior performance compared to the proposed method. Furthermore, the robustness of the proposed channel estimator is evaluated under imperfect knowledge of the intra-cell LSF coefficients, modeled as $\hat{\beta}_{ik}^{i} = \beta_{ik}^{i}\left(1 + \mathcal{N}(0, \sigma^2)\right)$, where σ^2 takes three values: 0.01, 0.001, and 0.0001. For $\sigma^2 = 0.01$, a noticeable performance degradation is observed at high SNR, whereas for $\sigma^2 = 0.001$, the impact is negligible. When $\sigma^2 = 0.0001$, the performance is nearly identical to that achieved by the proposed estimator, since the value of σ is very close to zero. Both analytical and simulation-based results are presented to validate the performance of the proposed estimator.

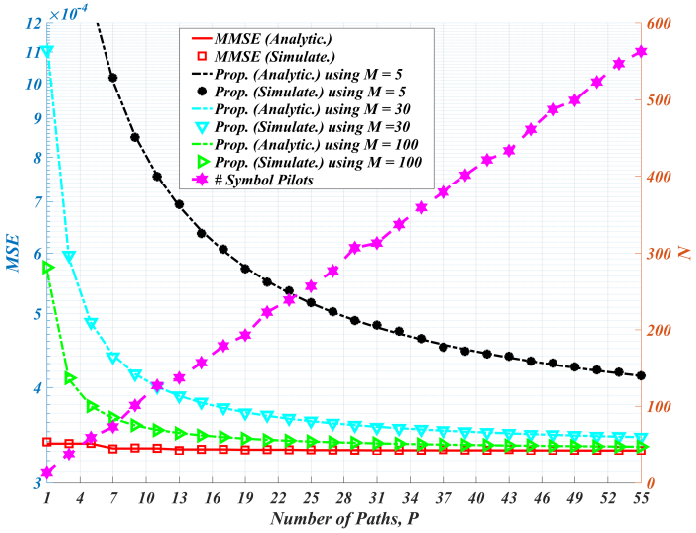

Figure 3. MSE as a function of pilot length S and number of paths P)

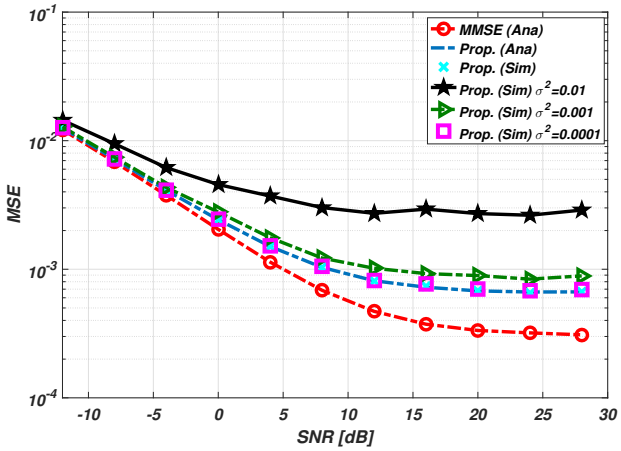

Figure 4. MSE as a function of SNR (dB) under imperfect knowledge of the intra-cell LSF coefficients

The simulation results illustrated in this study show that the implemented ML based channel estimator performs very close to the ideal MMSE estimator. This is done without relying on perfect LSF coefficients of the interfering users. This observation is particularly important for the design of M-MIMO systems in real-world scenarios where the full channel statistics are commonly unavailable. In comparison with other MMSE- and LS-based estimators, the proposed method strikes a favorable estimation accuracy and complexity balance, particularly in the presence of multipath propagation and in more realistic LoS scenarios. The given estimator's ability to extract needed parameters directly from the received signals diminishes the pilot and computation resources needed, the two main concerns in the state-of-the-art methods. The applied heuristic PoC also enhances CE in user-dense regions, which typically suffer from high inter-cell interference. Our method is different from previous works, which either assumed uniform PoC or required centralized control. Our work is novel in that it is simple and thus suitable for distributed or large-scale networks.

7. CONCLUSION

This study introduces a straightforward and computationally efficient channel estimator for TDD M-MIMO multipath communication. Unlike the conventional MMSE estimator, which relies on the impractical

assumption of a priori knowledge of the LSF coefficients of interfering users, the proposed approach operates under realistic propagation conditions, where channels may consist solely of NLoS components or a mix of LoS and NLoS paths depending on the user's distance from its serving BS. In addition, a heuristic PoC policy is developed to mitigate inter-cell interference for cell-edge users, particularly under the challenging case of frequency reuse factor 1. Analytical derivations and Monte Carlo simulations confirm that the proposed estimator achieves asymptotic performance comparable to the MMSE estimator, with strong agreement between theoretical and simulated results. Nevertheless, some limitations should be acknowledged. The proposed estimator assumes moderate user mobility, and its performance may degrade in highly dynamic scenarios where CSI changes rapidly. Similarly, the heuristic PoC scheme, while low in complexity, may not achieve globally optimal performance compared to more advanced optimization methods. Moreover, the adopted LoS/NLoS distance-based model provides a practical but simplified characterization of real propagation environments. Future research may extend this work to multi-cell and heterogeneous network deployments, integrate learning-based or hybrid statistical–ML estimators for improved robustness, and account for hardware impairments such as phase noise and non-linearities. Another promising direction is the design of adaptive and real-time power control strategies that respond to user mobility and traffic demand, thereby enhancing the practicality and efficiency of M-MIMO systems in real deployments.

Future directions: future study can extend this work in several directions: i) investigating the performance of the proposed estimator under mobility and dynamic LoS/NLoS transitions, ii) exploring hybrid methods that combine elements of blind estimation with the proposed approach for even greater pilot reduction, iii) adapting the proposed scheme for DL CE in FDD systems, which remains a challenge in M-MIMO, and iv) evaluating the estimator's robustness in hardware-impaired or imperfect synchronization environments.

FUNDING INFORMATION

Authors state no funding involved.

AUTHOR CONTRIBUTIONS STATEMENT

This journal uses the Contributor Roles Taxonomy (CRediT) to recognize individual author contributions, reduce authorship disputes, and facilitate collaboration.

Name of Author	C	M	So	Va	Fo	I	R	D	O	E	Vi	Su	P	Fu
Jamal Amadid	✓	✓	✓		✓	✓	✓		✓	✓	✓	✓		
Asma Khabba	✓	✓	✓		✓	✓	✓	✓	✓	✓			✓	
Zakaria El Ouadi	✓	✓	✓		✓	✓	✓		✓	✓				
Lahcen Sellak	✓	✓		✓	✓	✓		✓	✓	✓	✓			
Abdelmouttalib Bousrout	✓	✓			✓	✓		✓	✓	✓				
Abdelouahab Zeroual	✓	✓			✓	✓			✓	✓	✓		✓	
Tole Sutikno	✓	✓	✓	✓	✓	✓			✓	✓			✓	✓

C : **C**onceptualization
M : **M**ethodology
So : **So**ftware
Va : **Va**lidation
Fo : **Fo**rmal Analysis
I : **I**nvestigation
R : **R**esources
D : **D**ata Curation
O : Writing - **O**riginal Draft
E : Writing - Review & **E**diting
Vi : **Vi**sualization
Su : **Su**pervision
P : **P**roject Administration
Fu : **Fu**nding Acquisition

CONFLICT OF INTEREST STATEMENT

Authors state no conflict of interest.

DATA AVAILABILITY

Data availability is not applicable to this paper as no new data were created or analyzed in this study.

REFERENCES

[1] Ö. Özdogan, E. Björnson, and E. G. Larsson, "Massive mimo with spatially correlated rician fading channels," *IEEE Transactions on Communications*, vol, 67, no. 5, pp. 3234–3250, 2019, doi: 10.1109/TCOMM.2019.2893221.

[2] N. R. Challa and K. Bagadi, "Design of large scale mu-mimo system with joint precoding and detection schemes for beyond 5g wireless networks," *Wireless Personal Communications*, vol. 121, pp. 1627–1646, 2021, doi: 10.1007/s11277-021-08688-6.

[3] A. Belhabib, J. Amadid, M. Boulourd, M. M. Hassani, and A. Zeroual, "Pilot contamination suppression based coordination in multi-cell massive mimo systems," *Wireless Personal Communications*, vol. 125, no. 2, pp. 1883–1894, 2022, doi: 10.1007/s11277-022-09638-6.

[4] J. Amadid, A. Belhabib, and A. Zeroual, "On channel estimation in cell-free massive mimo for spatially correlated channels with correlated shadowing under rician fading," *International Journal of Communication Systems*, vol. 35, no. 1, pp. 1-15, 2022, doi: 10.1002/dac.5011.

[5] M. Indoonundon and T. P. Fowdur, "Enhancing the error performance of 5g new radio using hierarchical and statistical qam," *Wireless Personal Communications*, vol. 125, pp. 1951–1972, 2022, doi: 10.1007/s11277-022-09642-w.

[6] A. Khabba, J. Amadid, S. Ibnyaich, and A. Zeroual, "Pretty-small four-port dualwideband 28/38 ghz mimo antenna with robust isolation and high diversity performance for millimeterwave 5g wireless systems," *Analog Integrated Circuits and Signal Processing*, vol. 112, no. 1, pp. 83–102, 2022, doi: 10.1007/s10470-022-02045-8.

[7] S. Hamid *et al.*, "Hybrid beamforming in massive mimo for nextgeneration communication technology," *Sensors*, vol. 23, no. 16, pp. 1-13, 2023, doi: 10.3390/s23167294.

[8] J. Mirzaei, S. ShahbazPanahi, F. Sohrabi, and R. Adve, "Hybrid analog and digital beamforming design for channel estimation in correlated massive mimo systems," *IEEE Transactions on Signal Processing*, vol. 69, pp. 5784–5800, 2021, doi: 10.1109/TSP.2021.3118492.

[9] P. S. Shrivastava, U. K. Malviya, M. Meshram, and U. S. Dewangan, "Efficiency of ultra-dense multi-tier future cellular networks for 5g: A survey," *Wireless Personal Communications*, vol. 122, pp. 3269–3291, 2022, doi: 10.1007/s11277-021-09049-z.

[10] T. Balachander and M. B. M. Krishnan, "Carrier frequency offset (cfo) synchronization and peak average power ratio (papr) minimization for energy efficient cognitive radio network (crn) for 5g wireless communication," *Wireless Personal Communications*, vol. 127, pp. 1–21, 2021, doi: 10.1007/s11277-021-08726-3.

[11] T. L. Marzetta, "Noncooperative cellular wireless with unlimited numbers of base station antennas," *IEEE Transactions on Wireless Communications*, vol. 9, no. 11, pp. 3590–3600, 2010, doi: 10.1109/TWC.2010.092810.091092.

[12] K. K. Vaigandla and N. Venu, "Survey on massive mimo: Technology, challenges, opportunities and benefits," *SSRN preprint*, 2021.

[13] E. G. Larsson, O. Edfors, F. Tufvesson, and T. L. Marzetta, "Massive mimo for next generation wireless systems," *IEEE Communications Magazine*, vol. 52, no. 2, pp. 186–195, 2014, doi: 10.1109/MCOM.2014.6736761.

[14] S. Ahmed, Y. Khan, and A. Wahab, "A review on training and blind equalization algorithms for wireless communications," *Wireless Personal Communications*, vol. 108, pp. 1759–1783, 2019, doi: 10.1007/s11277-019-06495-8.

[15] J. Jose, A. Ashikhmin, T. L. Marzetta, and S. Vishwanath, "Pilot contamination and precoding in multi-cell tdd systems," *IEEE Transactions on Wireless Communications*, vol. 10, no. 8, pp. 2640–2651, 2011, doi: 10.1109/TWC.2011.060711.101155.

[16] M. K. Saeed, A. Khokhar, and S. Ahmed, "Pilot contamination in massive mimo systems: Challenges and future prospects," in *2024 International Wireless Communications and Mobile Computing (IWCMC)*, Ayia Napa, Cyprus, 2024, pp. 1504-1509, doi: 10.1109/IWCMC61514.2024.10592426.

[17] J. Amadid, A. Khabba, Z. El Ouadi, and A. Zeroual, "Impacts of three-dimensional array over channel estimation for cell-free massive mimo considering spatially correlated channels," *Transactions on Emerging Telecommunications Technologies*, vol. 33, no. 12, 2022, doi: 10.1002/ett.4638.

[18] Z. El Ouadi *et al.*, "Pretty small low-cost bandpass filter using a single square open-loop resonator with a centered stub for WLAN/Bluetooth/ZigBee/RFID and ISM band applications." *Optical and Quantum Electronics* vol. 56, no. 6, p. 1005, Apr. 2024, doi: 10.1007/s11082-024-06946-y

[19] T. V. Chien and E. Björnson, *Massive mimo communications*, 5G Mobile communications, Wiley, 2017, pp. 342-364, doi: 10.1002/9781118979846.ch15.

[20] E. Björnson, J. Hoydis, and L. Sanguinetti, *Massive mimo networks: Spectral, energy, and hardware efficiency*, Foundations and Trends in Signal Processing, 2017.

[21] R. M. Asif, A. U. Rehman, S. Guizani, and H. Hamam, "Enhancing spectral efficiency in uplink/downlink channels of multi-cell massive mimo for 5g networks," *International Journal of Advanced and Applied Sciences*, vol. 11, no. 8, pp. 66–79, 2024, doi: 10.21833/ijaas.2024.08.008.

[22] V. Joshi, V. Mundhada, S. Singh, R. Narange, and K. Dhote, "A multicell multiuser mimo uplink for a finite-dimensional channel in ofdm system," in *Proceedings of International Conference on Industrial Instrumentation and Control (ICI2C) 2021*, Springer, 2022, pp. 379–388, 10.1007/978-981-16-7011-4_37.

[23] H. Yin, D. Gesbert, M. Filippou, and Y. Liu, "A coordinated approach to channel estimation in large-scale multiple-antenna systems," *IEEE Journal on Selected Areas in Communications*, vol. 31, no. 2, pp. 264–273, 2013, doi: 10.1109/JSAC.2013.130214.

[24] S. G Gollagi, S. S. Maheswari, P. V. Sapkale, and S. Poojitha, "Channel estimation for pilot contamination in massive mimo-noma system," *Journal of High Speed Networks*, vol. 30, no. 3, pp. 355–373, 2024, doi: 10.3233/JHS-230043.

[25] T. L. Marzetta and H. Q. Ngo, *Fundamentals of massive MIMO*, Cambridge University Press, 2016, doi: 10.1017/CBO9781316799895.

[26] F. A. P. de Figueiredo, F. A. C. M. Cardoso, I. Moerman, and G. Fraidenraich, "Channel estimation for massive mimo tdd systems assuming pilot contamination and flat fading," *EURASIP Journal on Wireless Communications and Networking*, vol. 2018, no. 1, pp. 1–10, 2018, doi: 10.1186/s13638-018-1021-9.

[27] T. S. Rappaport, *Wireless communications: principles and practice*, Prentice hall PTR New Jersey, vol. 2, 1996.

[28] P. Tarafder, C. Chun, A. Ullah, Y. Kim, and W. Choi, "Channel estimation in 5g-and-beyond wireless communication: A comprehensive survey," *Electronics*, vol. 14, no. 4, pp. 1-19, 2025, doi: 10.3390/electronics14040750.

[29] D. Joann and V. Rajamani, "Evaluating mimo and massive mimo performance with rayleigh, rician, and nakagami fading channels along with comparing half-duplex and full-duplex modes using hmr protocol," *Innovation in MIMO Technologies, Systems, and*

Antennas, 2024, doi: 10.5772/intechopen.1008175.
[30] N. Shariati, E. Björnson, M. Bengtsson, and M. Debbah, "Low-complexity polynomial channel estimation in large-scale mimo with arbitrary statistics," *IEEE Journal of Selected Topics in Signal Processing*, vol. 8, no. 5, pp. 815-830, Oct. 2014, doi: 10.1109/JSTSP.2014.2316063.
[31] F.A. P. de Figueiredo, D.A. M. Lemes, C. F. Dias, and G. Fraidenraich, "Massive mimo channel estimation considering pilot contamination and spatially correlated channels," *Electronics Letters*, vol. 56, no. 8, pp. 410–413, 2020, doi: 10.1049/el.2019.3899.
[32] Z. Albataineh, N. Al-Zoubi, and A. Musa, "Channel estimation for massive mimo system using the shannon entropy function," *Cluster Computing*, vol 26, pp. 3793–3801, 2022, doi: 10.1007/s10586-022-03783-0.
[33] M. J. L. Morales, K. Chen-Hu, and A. G. Armada, "Pilot-less massive mimo tdd system with blind channel estimation using non-coherent dmpsk," in *GLOBECOM 2022-2022 IEEE Global Communications Conference*, Rio de Janeiro, Brazil, 2022, pp. 693-698, doi: 10.1109/GLOBECOM48099.2022.10000841.
[34] J. F Arellano, C. D. Altamirano, H. R. C. Mora, N. V. O. Garzón, and F. D. A. García, "On the performance of mmse channel estimation in massive mimo systems over spatially correlated rician fading channels," *Wireless Communications and Mobile Computing*, vol. 2024, no. 1, 2024.
[35] B. Dessie, J. Shaikh, G. Iliev, M. Nenova, U. Syed, and K. K. Kumar, "Performance evaluation of uplink cell-free massive mimo network under weichselberger rician fading channel," *Mathematics*, vol. 13, no. 14, pp. 1-20, 2025, doi: 10.3390/math13142283.
[36] 3rd generation partnership project, technical specification group radio access network, "Spatial channel model for multiple input multiple output (mimo) simulations," *3GPP TR 25.996* V14.0.0, 2017.
[37] T. L. Marzetta, "How much training is required for multiuser mimo?," in *2006 Fortieth Asilomar Conference on Signals, Systems and Computers*, Pacific Grove, CA, USA, 2006, pp. 359-363, doi: 10.1109/ACSSC.2006.35476.
[38] G. Caire, N. Jindal, M. Kobayashi, and N. Ravindran, "Multiuser mimo achievable rates with downlink training and channel state feedback," *IEEE Transactions on Information Theory*, vol. 56, no. 6, pp. 2845-2866, Jun. 2010, doi: 10.1109/TIT.2010.2046225.
[39] B. Sklar, "Rayleigh fading channels in mobile digital communication systems. i. characterization," *IEEE Communications Magazine*, vol. 35, no. 9, pp. 136-146, Sep. 1997, doi: 10.1109/35.620535.
[40] E. Dahlman, S. Parkvall, and J. Skold, *4G, LTE-advanced Pro and the Road to 5G*, Academic Press, 2016.
[41] D. Chu, "Polyphase codes with good periodic correlation properties (corresp.)," *IEEE Transactions on Information Theory*, vol. 18, no. 4, pp. 531-532, Jul. 1972, doi: 10.1109/TIT.1972.1054840.
[42] J. G. Andrews, "A primer on zadoff chu sequences," *arXiv preprint*, 2022, doi: 10.48550/arXiv.2211.05702.
[43] 3rd generation partnership project technical specification group radio access network, "Evolved universal terrestrial radio access (e-utra) physical channels and modulation," *3GPP TS 36.211* V11.0.0, Release 11, 2012.
[44] S. M Kay, "Fundamentals of statistical signal processing," Prentice Hall PTR, 1993.

BIOGRAPHIES OF AUTHORS

Jamal Amadid received the Ph.D. degree in Telecommunication, Electronics and Signal Processing from Cadi Ayyad University of Marrakech, Morocco in November 2022. The Thesis title is about the CE for M-MIMO in a more Practical Propagation Environment for 5th and 6th Generation of Wireless Communication Systems. He received a B.S. degree in Electronics in 2018 from the Cadi Ayyad University, Marrakech, Morocco. In 2020, he received the M.S. degree in Control, Industrial Computer, Signals, and Physical Systems from Cadi Ayyad University of Marrakesh, Morocco. He is currently a full time Professor at Higher Institute of Engineering and Business (ISGA), Marrakesh, Morocco. His research interests include telecommunication, electronics, signal processing, computer science, and wireless communications. He has published more than 23 conference papers, 9 book chapter and more than 16 journal papers. He can be contacted at email: j.amadid1297@uca.ac.ma or m.jamal.amadid@gmail.com.

Asma Khabba earned her Ph.D. in Telecommunication, Electronics, and Signal Processing from Cadi Ayyad University, Marrakech, Morocco, in 2024. Her doctoral research focused on Antenna Design for 5G wireless applications. She obtained her Bachelor's degree in Electronics from Cadi Ayyad University in 2015, followed by a Master's degree in Control, Industrial Computing, Signals, and Physical Systems in 2017 from the same institution. Currently, she serves as a full-time Professor at the Moroccan School of Engineering Sciences (EMSI) in Marrakech. Her research interests span telecommunications, electronics, 5G technologies, patch antenna, MIMO antennas, phased array antennas, and Thz antennas. Over her academic career, she has contributed extensively to the field through numerous conference presentations, book chapters, and journal publications. She can be contacted at email: khabba.asma@gmail.com.

Zakaria El Ouadi received a B.S. degree in Electronics in 2018 from the Cadi Ayyad University, Marrakech, Morocco. In 2020, he received the M.S. degree in Control, Industrial Computer, Signals, and Physical Systems from Cadi Ayyad University of Marrakesh, Morocco. He is currently a Ph.D. student in Telecommunications Engineering at the Cadi Ayyad University of Marrakesh, Morocco. His main research interest includes the filter nozzle design for 5G applications. He can be contacted at email: zakaria.elouadi@edu.uca.ac.ma.

Lahcen Sellak received his Bachelor's degree in Physics from the Ibn Zohr University, Agadir, Morocco and his Master's degree in Computer Control, Signals and Industrial Systems from Faculty of Sciences Semlalia, Cadi Ayyad University, Marrakech, Morocco in 2017 and 2019, respectively. Currently, he is actively pursuing a Ph.D. degree in Electronics, Telecommunications and Artificial Intelligence at the National School of Applied Sciences, Ibn Zohr University. His research interests include 5G antennas, microwave/millimeter antennas, array antennas, MIMO antennas, and the application of artificial intelligence techniques. He can be contacted at email: lahcensellak17@gmail.com.

Abdelmouttalib Bousrout received a specialized Master's degree in Telecommunication Systems at Ibn Tofail University in 2021 after earning a Bachelor of Physics degree with an electronics concentration from Cadi Ayyad University in 2018. He is currently pursuing her doctorate in signal processing and telecommunication at Ibn Tofail University in Kenitra, Morocco. Two of his main areas of interest are miniaturization and the development of high-performing antennas for biomedical applications. He can be contacted at email: abdelmouttalib1995@gmail.com.

Abdelouhab Zeroual is a professor of Telecommunication Systems and Signal Processing. He is the head of the Instrumentation, Signals, and Systems Team at the Faculty of Sciences Semlalia, Cadi Ayyad University in Marrakesh, Morocco. He received his Ph.D. degree in 1995 from Cadi Ayyad University. He supervises several research projects and serves as a reviewer for a number of international journals. His research interests include instrumentation, solar energy, signal processing, and wireless communications. He has published more than 140 conference papers and more than 60 journal papers. He can be contacted at email: zeroual@uca.ac.ma.

Prof. Ir. Tole Sutikno, Ph.D., MIET, IPM., ASEAN Eng. is a full professor in the Department of Electrical Engineering at Universitas Ahmad Dahlan (UAD) in Yogyakarta, Indonesia. He has held this position since 2023, having previously served as an associate professor from 2008. He earned his bachelor's degree from Universitas Diponegoro in 1999, his master's degree from Universitas Gadjah Mada in 2004, and his Ph.D. in Electrical Engineering from Universiti Teknologi Malaysia in 2016, where his doctoral research focused on advanced digital power electronics and intelligent control systems. From 2016 to 2021, he served as the Director of the Institute for Scientific Publishing and Publications (LPPI) at UAD, where he led initiatives to strengthen research visibility, journal management, and international collaboration in scholarly publishing. Since 2024, he has served as the head of the master's program in electrical engineering at UAD, following his leadership of the undergraduate program in electrical engineering in 2022. He is also the founding leader of the Embedded Systems and Power Electronics Research Group (ESPERG), which actively collaborates with both national and international institutions on topics such as fault-tolerant embedded systems, FPGA-based control, and renewable energy integration. He is widely acknowledged for his contributions to digital design, industrial electronics, motor drives, robotics, intelligent systems, and AI-based automation. His interdisciplinary research emphasises practical deployments in industrial and healthcare contexts, covering FPGA applications, embedded systems, power electronics, and digital libraries. He has published 380 peer-reviewed articles in high-impact journals and conferences indexed by Scopus. As of 2025, Google Scholar indicates over 6,000 citations, with an h-index of 36 and an i10-index of 174. In recognition of his global research impact, he has been listed among the Top 2% of Scientists Worldwide by Stanford University and Elsevier BV from 2021 to the present, a distinction based on standardised citation metrics across all scientific disciplines. He can be contacted at email: tole@te.uad.ac.id.